Chemical and Process Engineering 2014, 35 (1), 3-18
DOI: 10.2478/cpe-2014-0001

ANALYSIS OF THE LIQUID FLOW IN A VESSEL WITH A ROTATING DISK AT THE LIQUID SURFACE

Witold Suchecki*

Warsaw University of Technology, Płock Campus, Institute of Mechanical Engineering, Department of Process Equipment, Jachowicza 2/4, Płock, Poland

This study is concerned with liquid flow induced by a disk which rotates steadily around its axis and touches the free surface of liquid contained in a cylindrical vessel. It is a simplified model of the flow in the inlet part of a vertical cooling crystallizer where a rotary distributor of inflowing solution is situated above the free surface of solution contained in the crystalliser. Numerical simulations of flow phenomena were conducted and the simulation results were interpreted assuming an analogy with Kármán's theoretical equations. In a cylindrical coordinate system, the components of flow velocity were identified as functions of distance from the surface of the rotating disk. The experimental setup was developed to measure velocity fields, using digital particle velocimetry and optical flow. Conclusions concerning the influence of disc rotation on liquid velocity fields were presented and the experimental results were found to confirm the results of numerical simulation. On the basis of simulation data, an approximation function was determined to describe the relationship between the circumferential component of flow velocity and the distance from the disk.

Keywords: liquid flow, rotating disk, von Kármán's equations, velocity field, digital particle image velocimetry

1. INTRODUCTION

At the present state of knowledge it is often impossible to analyse precisely hydrodynamic phenomena which occur in liquids flowing through industrial apparatuses. This contributes to the designs of these apparatuses often being far from optimal. In principle, laboratory-scale research can be used to specify ways of forming the liquid flow in apparatuses so as to achieve uniform parameters of the liquid inside the outflowing stream. However, under industrial conditions and with typical apparatus designs it is usually impossible to measure such significant flow characteristics as flow-velocity fields in liquids, or to identify areas in which the flow is stagnant. As undetected non-uniform flow may unfavourably influence the process performed in the apparatus, finding flow characteristics is the key factor for apparatus optimisation.

In the various pieces of equipment used in chemical and food industries, single- or multiphase axisymmetrical flows occur, due to the influence of the shape of apparatus (e.g. in cyclones, hydrocyclones, etc.) and/or rotary movement of its parts (e.g. in settling centrifuges, stirred tanks, etc.). The important research problem is to identify the flow structures that are forming inside such apparatuses in order to acquire a firm understanding of flow phenomena as well as of their potential modifications which can improve process conditions (Suchecki, 2006).

*Corresponding author, e-mail: suchecki@pw.plock.pl

Rotary liquid flow in a cylindrical tank is an issue of significant interest in various fields of engineering and has been considered by numerous researchers. For example, liquid motion caused by the rotation of a cylindrical tank and liquid motion induced by a rotating disk placed on the free surface of liquid were studied through experimental research and numerical simulations (Escudier, 1984; Hyun et al., 1983; Lugt and Abboud, 1987; Patankar, 1980; Sørensen and Christensen, 1995; Warn-Varnas et al., 1978). The liquid flow in a rotating cylindrical tank with independently rotating disk placed on the liquid surface, that is, a combination of the two flows mentioned above, was analysed for Czochralski-type crystal growth processes. After performing experimental research at low values of the Reynolds number, Carruthers and Nassau (1968) described the effects of a relative change of the direction of rotation and the sizes of disk and tank on the flow field. Jones (1983) identified six various flow situations caused by thermal gradient and rotation at high values of the Reynolds number and the Grashof number and investigated velocity fields using flow visualisation. In a qualitative investigation, Ogino et al. (1993) used the LDV (Laser-Doppler Velocimetry) method to measure the distribution of flow velocity in a rotating cylindrical tank with a stationary disk placed on the free surface of liquid. Numerical simulations of liquid flow in Czochralski-type crystal growth processes were carried out for stationary flow at low values of the Reynolds number (Langlois, 1977). Furthermore, Mihelčić et al. (1982) simulated the large-scale Czochralski flow assuming boundary conditions with wall slip and no shear stress at the vessel wall.

Ruiz et al. (1991) examined the effect of boundary conditions using an identical flow model for a concentric disk-tank system in which both the disk and tank rotate. In the work of Inamuro et al. (1997), numerical simulation was conducted to identify flow-velocity fields in a rotating cylindrical tank with a coaxially rotating disk placed on the free surface of liquid. Axisymmetric Navier-Stokes equations were solved using the finite volume method. The effects of the relative direction of rotation and rotational speed of the disk and tank on the flow-velocity field in the liquid were investigated. In order to verify the accuracy of numerical simulation, its results were compared with the experimental data reported by Ogino et al. (1993).

Jasmine and Gajjar (2005) investigated the stability of numerical solutions of flow equations for an incompressible liquid contained between a rotating disk and a stationary lid. They adopted the notion of absolute stability introduced by Lingwood (1997) and considered his results as a reference. Using linear stability analysis, Jasmine and Gajjar (2005) investigated the effect of distance between the disk and lid and found that by reducing the distance, the critical Reynolds number can be increased and an absolutely stable flow can be obtained. The stability of flows of a liquid contained between rotating and stationary disks surrounded by a stationary enclosure was also considered by Schouveiler et al. (2001).

When comparing details of the results of research cited above, a number of inconsistencies can be found indicating that rotary flows are difficult to investigate, especially at high values of the Reynolds number. In the determination of velocity fields induced by simultaneous rotation of both the disk and liquid-containing tank, the uncertainty of results depends on both the relative rotation velocity and relative rotation directions of the disk and tank.

In order to shed additional light on the modelling of rotary flows, the present work combines numerical simulation with the approach used in the analytical Kármán model (Landau and Lifshitz, 2000; von Kármán, 1921). A simple case of liquid flow induced by a disk which rotates while touching the free surface of liquid contained in a stationary cylindrical tank is considered. It is a simplified theoretical model of flow phenomena in the inlet part of a vertical crystalliser in which a rotary distributor of inflowing solution is positioned above the free surface of solution in the crystalliser vessel. The liquid flow is simulated and the simulation results are compared with experimental results obtained in an experimental setup where flow velocity fields in a model tank equipped with rotating disk are identified using flow visualisation and correlation-based methods of flow-image analysis, and the components of flow velocity are determined as functions of distance from the disk.

The aim of the present work is to determine how the flow velocity, induced by disk rotation at the free surface of liquid contained in a cylindrical vessel, changes with increasing distance from the disk. Using numerical results generated by the validated simulation model, approximation functions are sought assuming analogy with functions introduced by Kármán in his theoretical model which is summarised below. The approximation functions are expected to constitute a simple engineering tool making it possible, for known vessel and disk dimensions and rotational speed of the disk, to determine the distance from the disk at which the rotary liquid flow decays.

2. RIGOROUS SOLUTION OF THE EQUATION OF VISCOUS LIQUID FLOW

An infinite flat disk rotating at a constant angular velocity ω is immersed in a viscous liquid. The distribution of liquid-flow velocity induced by the disk needs to be specified (von Kármán, 1921).

The disk surface is selected as the plane z = 0 in cylindrical coordinates (r, φ, z). Assuming that the liquid is bounded by its free surface only, the boundary conditions for flow velocity components are as follows:

$$\begin{aligned} &V_r = 0, \quad V_\varphi = \omega \cdot r, \quad V_z = 0 \quad \text{for} \quad z = 0, \\ &V_r = 0, \quad V_\varphi = 0, \quad V_z = 0 \quad \text{for} \quad z = \infty. \end{aligned} \tag{1}$$

As the liquid in the vicinity of the disk flows in a radial direction away from the rotation axis, then in accordance with the continuity equation, an axial component of the flow velocity directed from infinity to the disk surface must exist. At $z \to \infty$, axial velocity V_z approaches a constant value determined by the flow equations. The solution of flow equations is assumed in the following form:

$$\begin{aligned} &V_r = r\omega F(z_1), \quad V_\varphi = r\omega G(z_1), \quad V_z = \sqrt{\nu\omega}\, H(z_1), \\ &\text{where} \quad z_1 = \sqrt{\frac{\omega}{\nu}}\, z. \end{aligned} \tag{2}$$

It is assumed that both radial velocity V_r and circumferential velocity V_φ are proportional to the distance from the axis of disk rotation and axial velocity V_z is constant over each horizontal plane.

By substituting the continuity equation into the Navier-Stokes equation, the following equations are obtained for functions F, G, H (quotation marks indicate differentiation with respect to z_1):

$$\begin{aligned} &F^2 - G^2 + F'H = F'', \quad 2FG + G'H = G'', \\ &HH' = P' + H'', \qquad 2F + H' = 0 \end{aligned} \tag{3}$$

with boundary conditions:

$$\begin{aligned} &F = 0, \quad G = 1 \quad \text{for} \quad z_1 = 0, \\ &F = 0, \quad G = 0 \quad \text{for} \quad z_1 = \infty. \end{aligned} \tag{4}$$

The problem is thus reduced to the integration of a system of differential equations in one variable and can be solved numerically (see Fig. 1). The value of function H at $z \to \infty$ equals –0.886; in other words, the velocity of liquid flowing from infinity towards the disk is $V_z(\infty) = -0.886 \cdot \sqrt{\nu\omega}$.

The known functions F, G and H make it possible to express the three components of flow velocity: radial $V_r = r\omega \cdot F(z_1)$, circumferential $V_\varphi = r\omega \cdot G(z_1)$, and axial $V_z = \sqrt{\nu\omega} \cdot H(z_1)$, as functions of the dimensionless distance from the rotating disk z_1.

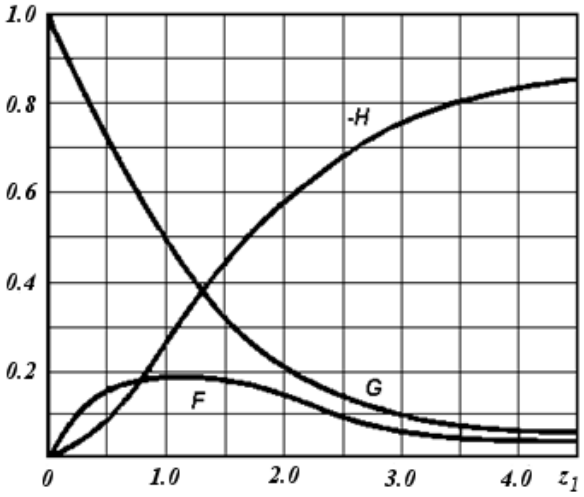

Fig. 1. Diagram of functions *F*, *G*, *-H*

3. SIMULATION MODEL

To simulate a liquid flow induced by a rotating disk placed at the free liquid surface, CFD software package *Fluent 6.0* was selected. In the first step, a geometrical model was created and a corresponding CFD grid was generated using *Gambit 2.0* software. After that, boundary conditions and initial conditions were identified, physicochemical properties of the liquid defined, equations of the mathematical model formulated and the problem-solving approach chosen using *Fluent 6.0*.

3.1. Computational model

The model geometry is presented in Fig. 2. A cylindrical vessel 90 mm in diameter and 240 mm in height is filled with glycerol up to the level of 200 mm. Inside the vessel, a disk which can rotate at various speeds is positioned in contact with the liquid surface. The disk is 5 mm thick and 50 mm or 70 mm in diameter. Its rotational speed is in the range of 2.51 to 12.06 rad/s. The properties of glycerol are as follows:

- dynamic viscosity $\mu = 1.198$ Pa·s,
- density $\rho = 1473$ kg/m^3,
- kinematic viscosity $\nu = 8.13 \cdot 10^{-4}$ m^2/s.

It should be stressed that the model geometry, liquid properties and speeds of the disk rotation were assumed to match the specifications of the experimental setup, thus making it possible to compare simulation results with experimental data.

3.2. Numerical grids and boundary conditions

Numerical simulations were conducted in 2D and 3D using *Fluent* software. In 2D simulations, only the area marked by thick lines in Fig. 2 was considered since the computational model is axisymmetrical.

The two-dimensional grid was uniform over the whole flow area. It consisted of square elements 0.5 mm by 0.5 mm and its characteristic data were: number of cells 36000, minimum orthogonal quality 1, maximum aspect ratio 1.41. The three-dimensional grid consisted of pyramid elements and

the grid density was the highest in the vicinity of the disk and the lowest at the bottom of the vessel; number of cells 1425185, minimum orthogonal quality 0.276, maximum aspect ratio 16.2.

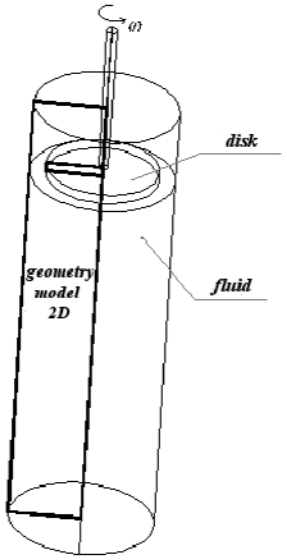

Fig. 2. Geometry of the computational model

Similar to the Kármán model, disk rotation around its axis (coordinate z) at angular velocity ω is assumed. Contrary to that model, the liquid is bounded not only by its free surface, but also by the vessel walls. In the basic case ("model without free surface"), the boundary conditions are following:

$$\begin{aligned} &V_r = 0, \quad V_\varphi = \omega \cdot r, \quad V_z = 0 \quad \text{for} \quad z = 0, \\ &V_r = 0, \quad V_\varphi = 0, \quad V_z = 0 \quad \text{for} \quad z = h, \end{aligned} \tag{5}$$

where h – distance between the disk and vessel bottom.

As an option („model with free surface"), the existence of a gas which can influence the flow of liquid in the region adjacent to its free surface is assumed and reflected by an additional boundary condition.

4. EXPERIMENTAL

4.1. Experimental setup

A cylindrical vessel 90 mm in diameter and 240 mm high was filled with liquid to a level of 200 mm. Two disks were used, 50 mm and 70 mm in diameter and 5 mm thick. When touching the free surface of the liquid, each disk rotated with angular velocities in the range ω = 1.3–4.6 1/s (rotational speed 1.05−4.61 rad/s). Throughout all experiments, the liquid was a mixture of water and glycerol with a dynamic viscosity of μ = 1.198 Pa·s and density of ρ = 1473 kg/m^3.

The experimental setup is schematically shown in Fig. 3. Above the free surface of the liquid contained in vessel 1, disk 3 was driven by variable-speed DC motor 5. Images of the flow of liquid with trace particles (Raffel et al., 1998; Westerweel, 1993) added were captured by digital camera 2 placed below the vessel. Two cameras were used: HCC1000 with a resolution of 768×576 pixels or Basler A102f, 1392×1040 pixels.

In order to eliminate the risk of deformation of flow images, the vessel was placed in optical envelope 7 formed of a cubicoidal container filled with the same liquid (without trace particles). Light source 6 and

camera 2 were both mounted on a console which could be moved vertically enabling to investigate the liquid flow in vessel cross-sections positioned at variable distance from the free surface of the liquid.

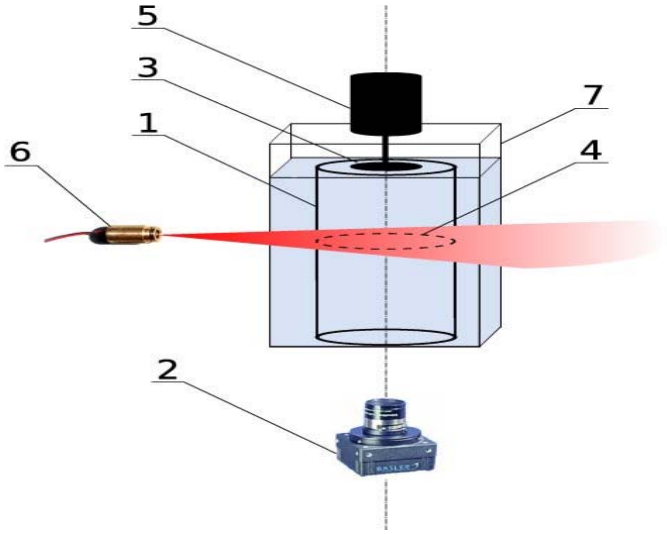

Fig. 3. Scheme of the experimental setup,
1 – vessel, 2 – camera, 3 – disk, 4 – light sheet, 5 – variable-speed DC motor, 6 – light source,
7 – optical envelope

4.2. Processing of experimental data

Sets of consecutive flow images captured by the camera and recorded during the experiments were processed using the methods of digital particle image velocimetry (Raffel et al., 1998; Westerweel, 1993) and optical flows (Quénot et al., 1998). After processing, a set of consecutive images is converted into sets of particle-displacement maps and flow-velocity maps.

The flow diagram of the processing of experimental data is shown in Fig. 4. Except for the visualisation of velocity-vector maps, the processing of data was implemented under Linux using widely accessible software (Coriander, Gimp), in-house programs (dpiv (Suchecki, 2000), FUS (Suchecki, 2003)), and programs made available by the Institute of Fundamental Technological Research in Warsaw (opflow, img2bmp). The maps of velocity vectors were generated using Tecplot software under Windows.

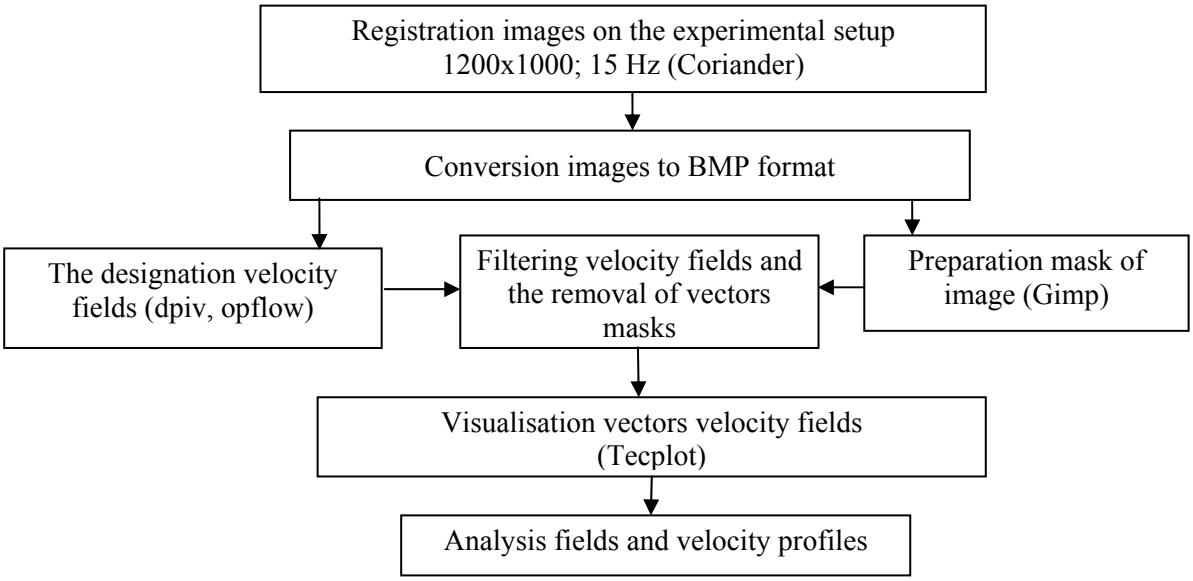

Fig. 4. Flow diagram of the processing of experimental flow images

Flow velocity fields were recorded by sequential positioning of the light sheet in vessel cross-sections spaced 10 mm apart in the depth range 0–100 mm and in the longitudinal section. At a fixed disk diameter and its rotational speed, a complete set of data on the three-dimensional velocity field included two-dimensional flow maps obtained for all the cross-sections and the longitudinal section. By varying the rotational speed, 18 data sets were generated for each of the two disk diameters. An example of graphical representation of the three-dimensional liquid flow, in the entire vessel volume, by several two-dimensional flow velocity contours is shown in Fig. 5.

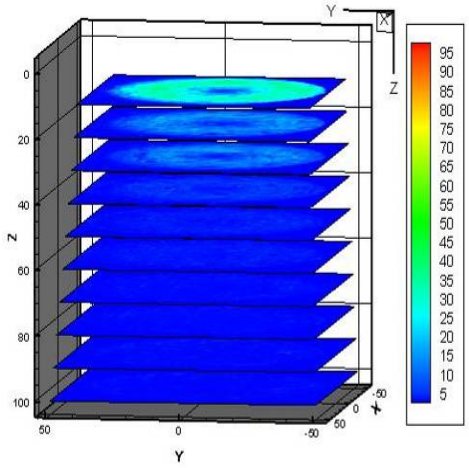

Fig. 5. Contours of flow velocity in a selected cross section of the vessel obtained for 70 mm disk rotated at 4.61 rad/s. Values of distance along coordination axes are given in mm and values of flow velocity – in mm/s

5. SIMULATION RESULTS

Various problem-solving approaches were tested with the aim to identify those which combine modest computational effort with reasonable accuracy. In order to evaluate the accuracy of modelling, the simulation results were experimentally verified using digital particle image velocimetry (DPIV) and optical flows. The experimental results are presented in the section titled *Experimental results and comparison with simulation results*.

The best agreement between the results of experimental research and those of numerical modelling was found for the following models:

- 2D with free surface,
- 2D without free surface,
- 3D.

5.1. 2D models - with free surface and without free surface

The results of numerical simulation for 2D model without free surface were identical to those obtained using 2D model with free surface. The diameter and rotational speed of the disk exert a significant effect on the depth of the zone in which the liquid is affected by disk rotation. The bigger the diameter and rotational speed, the greater is the distance from the disk where the rotary flow of liquid decays.

Just below the disk, the circumferential velocity of the liquid flow at the rotation axis is zero but increases with the radius and is the highest in the vicinity of the disk edge. When moving down away from the disk, the flow velocity decreases rapidly and for practical purposes, it can be regarded as negligibly small if the maximum value of its circumferential component becomes smaller than 0.005 m/s (Suchecki, 2008). The distance from the disk where this condition is satisfied can be

determined on the basis of simulation results. For two values of the disk diameter and variable rotational speed of the disk, the values of distance from the disk where the maximum value of circumferential flow velocity is about 0.005 m/s are presented in Table 1.

Table 1. Distance z from the disk, and its dimensionless equivalent z/h (h = 200 mm is the distance between the disk and tank bottom), where the circumferential flow velocity becomes negligibly small. Disk diameters 50 mm and 70 mm, rotational speed 2.51–12.06 rad/s

Disk diameter [mm]	Rotational speed of the disk [rad/s]									
	2.51	4.45	4.95	6.85	7.49	9.30	9.48	10.71	10.89	12.06
	Dimensionless rotational speed (relative to 9.30 rad/s)									
	0.27	0.48	0.53	0.74	0.81	1.00	1.02	1.15	1.17	1.30
50	Distance from the disk [mm]									
	24	30.5	32	36	37	40	40.5	41.5	42	43.5
	z/h [-]									
	0.120	0.153	0.160	0.180	0.185	0.200	0.203	0.208	0.210	0.218
70	Distance from the disk [mm]									
	31	38	39	43	44.5	47	47.5	49.5	50	51
	z/h [-]									
	0.155	0.190	0.195	0.215	0.223	0.235	0.238	0.248	0.250	0.255

5.2. 3D model

The three-dimensional simulation was based on a model without free surface with boundary condition imposed on the shear stress between the disk and the vessel wall. The simulation results were presented in the form of flow velocity profiles and vectors fields, and diagrams depicting the distribution of flow velocity along the vessel radius in specific cross-sections of the vessel. Figure 6 presents flow velocity fields at the disk surface and in the cross section located 40 mm below the disk, obtained assuming disk diameter of 70 mm and rotational speed of 9.30 rad/s. The arrows visualise vectors of the horizontal component (i.e., the sum of radial and circumferential components) of flow velocity. The distribution of velocity vectors is typical for the rotary liquid flow.

Changes in the value of the horizontal component of flow velocity along the vessel radius in the cross-section which touches the disk surface are shown in Fig. 7. Owing to adhesion forces, the radial velocity is zero at the disk surface. The horizontal velocity is zero at the rotation axis, increases linearly with the radius attaining its maximum in the vicinity of disk edge, and subsequently decreases approaching zero at the surface of vessel wall.

Regarding vessel cross-sections below the disk, it was found that the distribution of flow velocity is more uniform than that in the cross-section close to the disk surface. Moving away from the vessel axis, the horizontal velocity increases attaining its maximum at a distance comparable with the disk radius and subsequently decreases approaching zero at the wall surface. For three selected cross-sections, the maximum value of the horizontal velocity together with the corresponding distance from the vessel axis is given in Table 2.

While comparing the distribution of velocity vectors in vessel cross-sections 20 mm, 40 mm and 60 mm below the disk surface, it was found that rotary liquid flow is maintained down to the depth of

40 mm. At 60 mm depth irregularities were detected in the distribution of vectors of horizontal flow velocity. This can be attributed to liquid circulation in the vessel.

Summing up the obtained results, the highest values and largest radial gradients of horizontal flow velocity were observed in the cross-section close to the disk surface. When moving deeper into the vessel, velocity values and radial velocity gradients decrease.

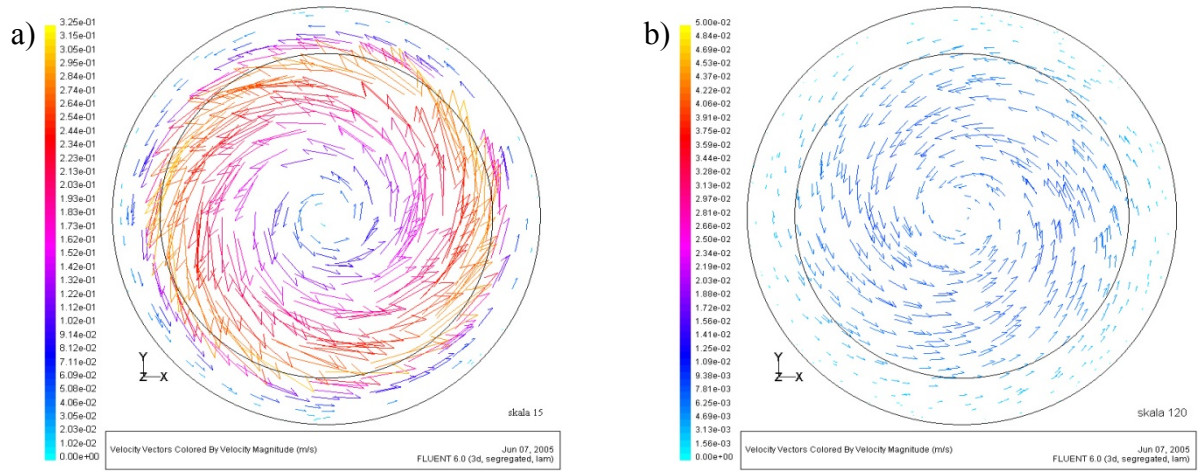

Fig. 6. Horizontal component of the flow velocity in two cross-sections of the vessel:
a) at the disk surface, b) 40 mm below the disk. Disk diameter 70 mm, rotational speed 9.30 rad/s

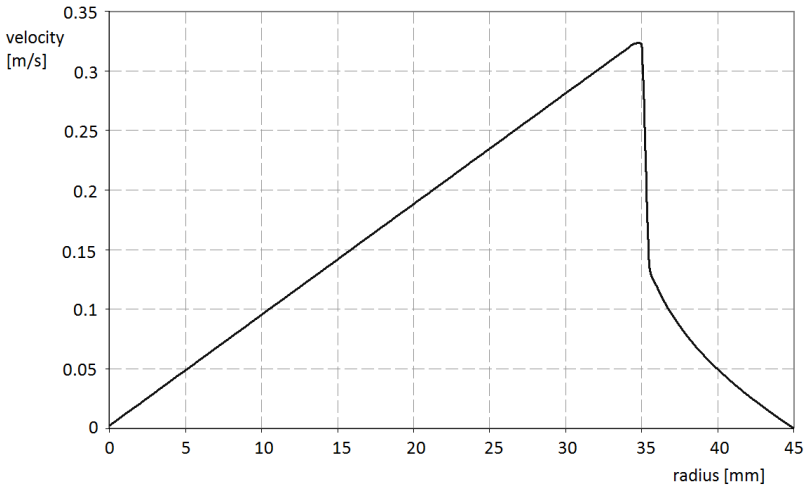

Fig. 7. Radial distribution of the horizontal component of the flow velocity in the cross-section of the vessel close to the disk surface ($z/h = 0$). Disk diameter 70 mm, rotational speed 9.30 rad/s

Table 2. Maximum values of the horizontal flow velocity in selected vessel cross-section below the disk. Disk diameter 70 mm, rotational speed 9.30 rad/s

Distance from disk surface [mm]	z/h [-]	Maximum horizontal velocity, [m/s]	Distance from vessel axis [mm]
20	0.1	0.045	25
40	0.2	0.009	21
60	0.3	0.0014	19

6. EXPERIMENTAL RESULTS AND COMPARISON WITH SIMULATION RESULTS

Experimentally obtained particle trajectories as well as flow velocity contours and vector maps were qualitatively compared with the corresponding outputs of numerical simulations. Regarding velocity fields, at increasing distance from the disk, the values of flow velocity are rapidly decreased. In the entire range of rotational speed of both disks (diameters 50 mm and 70 mm), the velocity values were negligibly small at 50 mm depth and below (see Fig. 10).

In general, the simulation results agree very well with the experimental ones. In Fig. 8, this is demonstrated by the vectors maps of horizontal flow velocities determined in a selected vessel cross-section. A representative radial distribution of the simulated and experimentally determined horizontal component of the flow velocity in the vessel cross-section close to the disk surface is shown in Fig. 9. For two different disks rotating at the same speed, changes in the simulated and experimentally determined circumferential component of the flow velocity along the distance from disk surface are shown in Fig. 10.

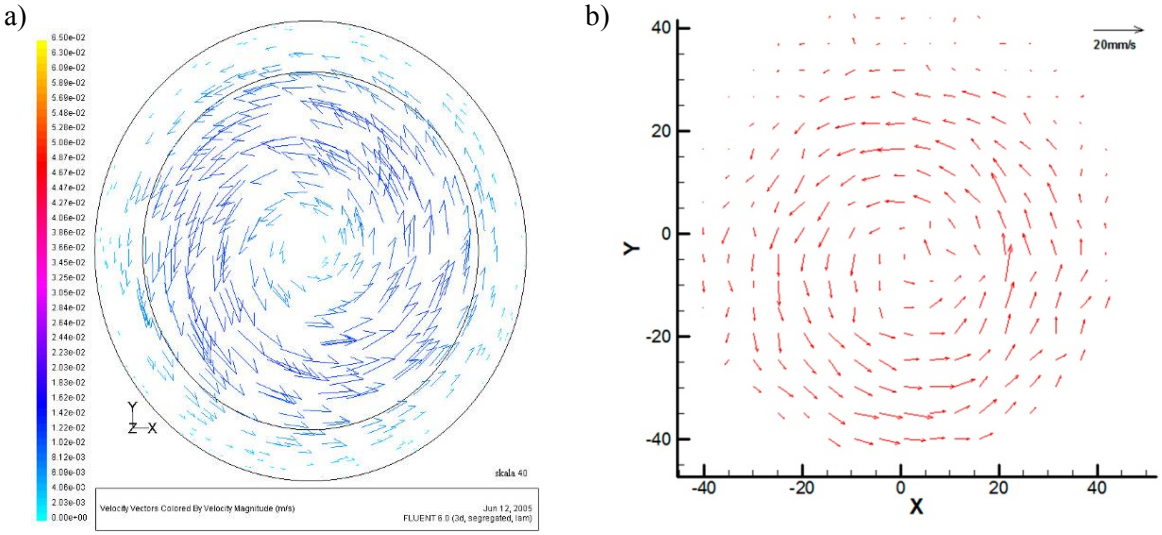

Fig. 8. Horizontal component of the flow velocity in the vessel cross-section 20 mm below the disk. Disk diameter 70 mm, rotational speed 2.62 rad/s. a) determined by simulation, b) determined by experiment

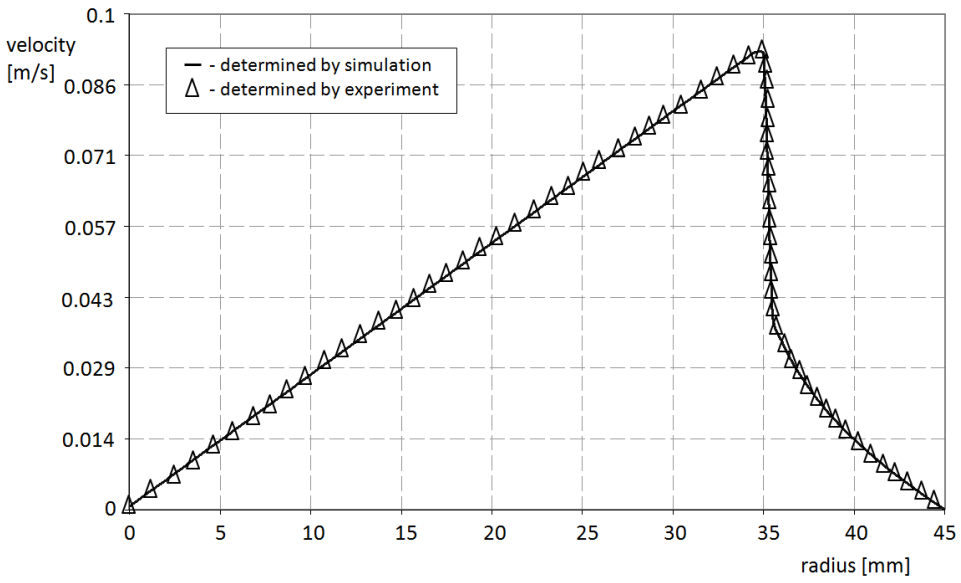

Fig. 9. Radial distribution of the horizontal component of the flow velocity in the cross-section close to the disk surface determined by simulation and by experiment. Disk diameter 70 mm, rotational speed 2.62 rad/s

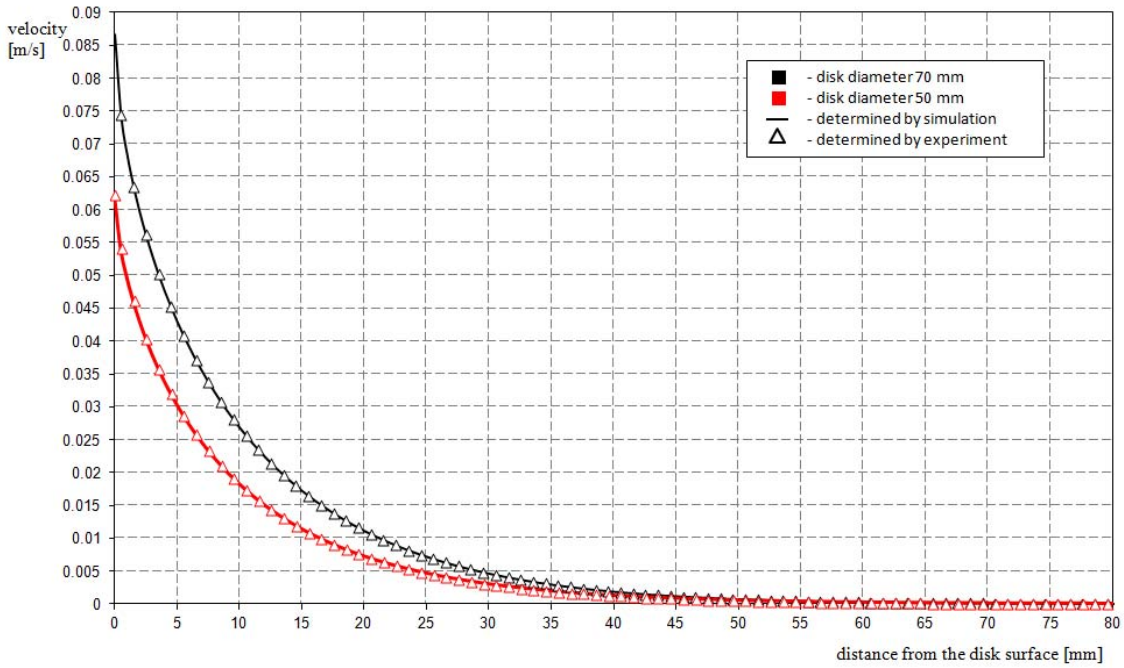

Fig. 10. Circumferential flow velocity at r = 22 mm determined by simulation and by experiment, as a function of the distance from disk surface. Disk diameter 50 mm (red line) and 70 mm (black line), rotational speed 2.62 rad/s

While the correctness of the numerical model is confirmed, the predictions obtained from the Kármán model deviate significantly from the experiment. It is understandable as the finite dimensions of the disk and vessel are not reflected in the model assumptions of infinitely large disk diameter and semi-infinite space filled with liquid.

In a vessel of finite dimensions, as the liquid in the vicinity of a rotating disk flows radially away from the rotation axis, liquid circulation in the vessel volume is unavoidable. As a consequence, vertical (axial) components of flow velocity must occur especially in the regions close to the vessel wall and disk rotation axis. This was experimentally confirmed but in the experiments performed with the mixture of water and glycerol, the values of vertical velocity were very small. The circulation of the liquid was more intensive in additional experiments performed with pure water as its viscosity is much smaller than that of the mixture. The vertical components of flow velocities in various parts of the vessel increased with increasing rotational speed of the disk. Secondary circulation was sometimes established in the bottom part of the vessel.

7. FLOW VELOCITY FIELDS DETERMINED BY NUMERICAL SIMULATION

Selected results of numerical simulations performed for the two-dimensional model with boundary condition between the disk and the vessel wall were expressed using three functions F_1, G_1 and H_1 analogous to those of the Kármán model. Most interesting is function G_1 as it can be helpful in estimating the depth at which the rotary flow decays.

The circumferential flow velocity was assumed to follow the equation

$$V_\varphi = r \cdot \omega \cdot G_1(z_1) \tag{6}$$

where $z_1 = z\sqrt{\frac{\omega}{\nu}}$.

In a vessel cross-section positioned at distance z below the disk surface, the flow velocity can be expressed as follows

$$V(z) = r \cdot \omega + a_o \cdot \left[1 - e^{-(a_1 \cdot z\sqrt{\omega/\nu})}\right] + a_2 \cdot \left[1 - e^{-(a_3 \cdot z\sqrt{\omega/\nu})}\right] \tag{7}$$

The values of approximation coefficients determined on the basis of simulation results obtained for disk diameters 70 mm and 50 mm are presented in Tab. 3.

Table 3. Approximation coefficients

Disk diameter [mm]	a_0	a_1	a_2	a_3
70	-0.187	27.324	-0.808	2.500
50	-0.224	24.223	-0.771	2.747

8. COMPARISON BETWEEN THE RESULTS OF NUMERICAL SIMULATIONS AND THOSE OF THE KÁRMÁN MODEL

The results presented below were obtained assuming the value of radial coordinate (distance from the vessel axis which is identical with the axis of disk rotation) r = 25 mm. Using simulation results obtained for different values of the disk diameter and rotational speed, the circumferential, radial and axial velocity components were identified as functions of distance from the disk. Next, functions $F_1(z_1)$, $G_1(z_1)$, $H_1(z_1)$ analogous to those introduced in the equation system (2) were determined and graphically presented as curves which can be compared with those shown in Fig. 1.

An example of diagram of function G_1 determined on the basis of simulation results is presented in Fig. 11a. The shape of the curve is similar to that of the corresponding curve shown in Fig. 1.

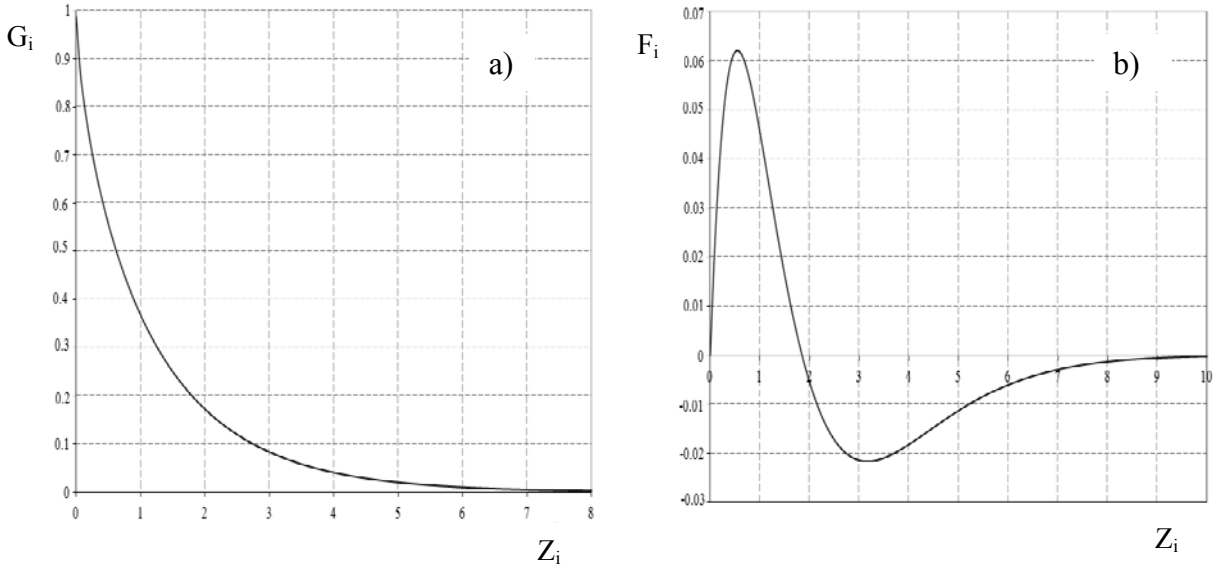

Fig. 11. Diagrams determined on the basis of results of numerical simulation at r = 25 mm: a) function G_1; b) function F_1. Disk diameter 70 mm, rotational speed 10.71 rad/s

The curve representing function F_1 (Fig. 11b) is similar to its theoretical analogue shown in Fig. 1 only for $z_1 < 2$. This is a consequence of liquid circulating in the region between the axis and the vessel wall. The radial component of flow velocity in the upper part of the vessel ($z_1 < 2$) is directed from the axis

to the wall, that is, its value is positive. In the bottom part ($z_1 > 2$), the direction of radial movement is reversed, that is, the value of radial velocity is negative. Contrary to that, in the theoretical Kármán model (i.e., liquid flow in a semi-infinite space) the radial component of flow velocity is always positive.

Another consequence of liquid circulation is that the curve representing simulation-based function H_1 (example in Fig. 12) is different from its theoretical analogue shown in Fig. 1. In the central part of the vessel around its axis, the axial component of flow velocity is directed upwards, that is, the value of H_1 is negative ($-H_1$ is positive). In the toroidal space close to the vessel wall, the axial velocity is directed downwards ($-H_1$ is negative). Contrary to that, in the theoretical Kármán model liquid flow from infinity to the disk is assumed so that the axial component of flow velocity is always positive.

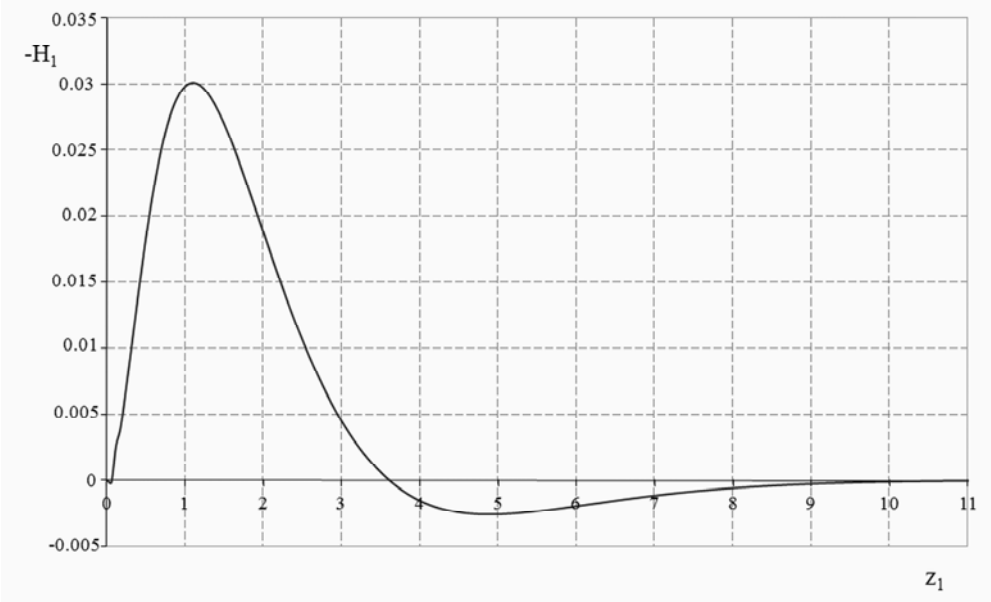

Fig. 12. Diagram of function H_1 determined on the basis of numerical simulation at $r = 25$ mm. Disk diameter 70 mm, rotational speed 10.71 rad/s

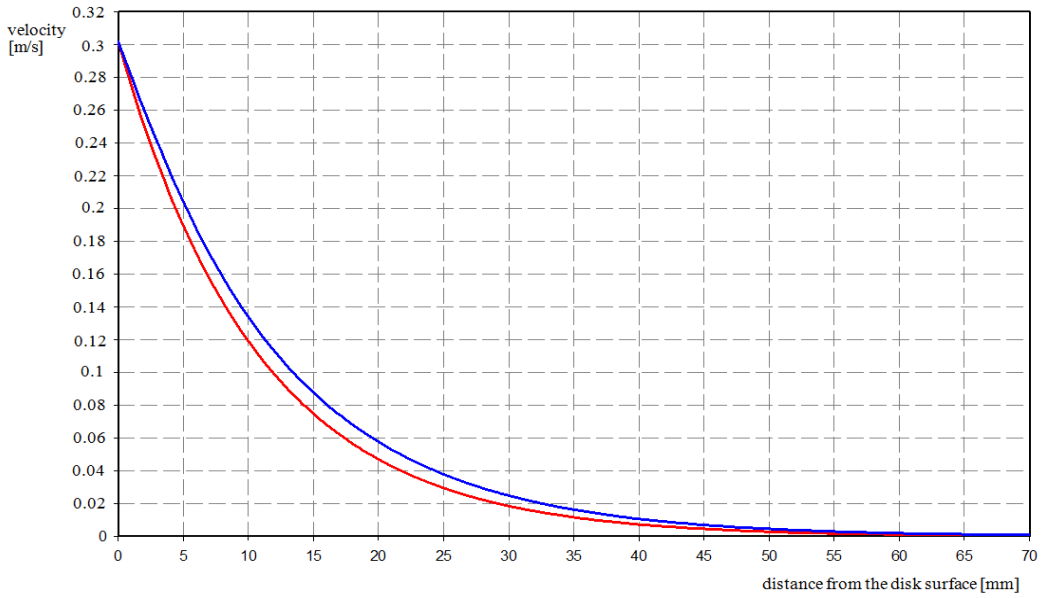

Fig. 13. Circumferential flow velocity at $r = 22$ mm estimated using the theoretical model (red line) and determined by simulation (blue line). Disk diameter 70 mm, rotational speed 12.06 rad/s

Bearing in mind that in the example illustrated in Fig. 12, the distance from the vessel (and disk rotation) axis is 25 mm, it can be concluded that on a cylindrical surface with the radius of 25 mm, in its upper part ($z_1 < 3.6$) the axial component of flow velocity is directed upwards but in its lower part ($z_1 > 3.6$), the direction of the axial component is reversed.

As a complement to the qualitative reasoning presented above, a comparison was made between the circumferential component of flow velocity determined by the numerical simulation (as a function of distance from the disk) and that estimated using the Kármán model. The calculations were performed assuming disk diameter to be 70 mm and rotational speed of 2.51 rad/s and 12.06 rad/s.

As can be seen in Fig. 13, the simulation results obtained for the rotational speed of 12.06 rad/s are close to the theoretical estimates. However, for the rotational speed of 2.51 rad/s large differences were observed between simulation results and theoretical estimates. For example, at a distance of 30 mm from the disk surface, the value of circumferential velocity obtained by simulation is greater than that estimated using the theoretical model by a factor of about 3.5 (difference 250%).

6. CONCLUSIONS

In the zone where liquid flow occurs, the flow velocity generally depends on the disk diameter and its rotational speed. At increasing rotational velocity, the flow velocity of the liquid is increased. Similarly, an increase in disk diameter causes the liquid flow velocity to increase. Furthermore, the diameter of the disk and its rotational velocity influence the distribution of flow velocity along the vessel axis. The bigger the diameter and rotational speed, the greater is the distance from the disk at which the rotary liquid flow decays. This relationship was determined by simulation and experimentally confirmed.

The results of numerical simulation agree with those based on the theoretical model only in the case of circumferential velocity V_φ. Regarding radial velocity V_r and axial velocity V_z, large discrepancies are observed. They are due to the difference between the simulation model, in which the diameter of the disk and dimensions of the liquid-containing vessel are finite, and the Kármán theoretical model, where infinitely large disk diameter and liquid flow in a semi-infinite space are assumed. However, taking advantage of similar features of both models, the circumferential component of flow velocity as a function of distance from the disk can be expressed by Equation (7). It stems from the Kármán model but includes coefficients which depend on the disk diameter and can be determined on the basis of simulation or experimental results. For known values of disk diameter and rotational speed, Equation (7) makes it possible to determine a_o at which distance from the disk, the circumferential component of flow velocity becomes negligibly small.

When choosing a numerical model one should aim at obtaining simulation results as close to reality as possible. On the basis of simulations conducted, it can be concluded that both the model with free liquid surface and the model without free surface produce results which are in good agreement with experimental data. However, the model without free surface is easier to use, and the associated computing time is shorter than that needed for the other model.

Meaningful discussions with Prof. Krzysztof Urbaniec are gratefully acknowledged.

SYMBOLS

a_0, a_1, a_2, a_3	approximation coefficients
F, G, H	functions describing the components of flow velocity: radial, circumferential and axial
r	disk radius, mm

z	distance from the disk, mm
V	velocity, m/s

Greek symbols

μ	dynamic viscosity, Pa·s
ν	kinematic viscosity, m^2/s
ρ	density, kg/m^3
ω	angular velocity of the disk, rad/s

Subscripts

r, φ, z	cylindrical coordinates

REFERENCES

Carruthers J.R., Nassau K., 1968. Nonmixing cells due to crucible rotating during Czochralski crystal growth. *J. Appl. Phys.,* 39, 5205-5214. DOI: 10.1063/1.1655943.

Escudier M.P., 1984. Observation of the flow produced in a cylindrical container by a rotating endwall. *Exp. Fluids*, 2, 189-196. DOI: 10.1007/BF00571864.

Hyun J.M., Leslie F., Fowlis W.W., Warn-Varnas A., 1983. Numerical solutions for spin-up from rest in cylinder. *J. Fluid Mech*., 127, 263-281. DOI: 10.1017/S0022112083002712.

Inamuro T., Yamaguchi A., Ogino F., 1997. Fluid flow in a rotating cylindrical container with a rotating disk at the fluid surface. *Fluid Dyn. Res*., 21, 417-430. DOI: 10.1016/S0169-5983(97)00020-8.

Jasmine H.A., Gajjar J.S.B., 2005. Absolute instability of the von Kármán, Bödewadt and Ekman flows between a rotating disc and a stationary lid. *Phil. Trans. R. Soc*. A, 363, 1131-1144. DOI: 10.1098/rsta.2005.1555.

Jones A.D.W., 1983. An experimental model of the flow in Czochralski growth. *J. Cryst. Growth*, 61, 235-244. DOI: 10.1016/0022-0248(83)90360-3.

Landau L.D., Lifshitz J.M., 2000. *Fluid Mechanics, Volume 6 of course of theoretical physics.* Butterworth-Heinemann, New Delhi.

Langlois W.E., 1977. Digital simulation of Czochralski bulk flow in a parameter range appropriate for liquid semiconductors. *J. Cryst. Growth*, 42, 386-399. DOI: 10.1016/0022-0248(77)90222-6.

Lingwood R.J., 1997. Absolute instability of the Ekman layer and related rotating flows. *J. Fluid Mech*., 331, 405–428. DOI: 10.1017/S0022112096004144.

Lugt H., Abboud M., 1987. Axisymmetric vortex breakdown with and without temperature effects in a container with a rotating lid. *J. Fluid Mech*., 179, 179-200. DOI: 10.1017/S0022112087001484.

Mihelčić M., Schroeck-Pauli C., Wingerath K., Wenzl H., Uelhoff W., Van Der Hart A., 1981. Numerical simulation of forced convection in the classical Czochralski method in ACRT and CACRT. *J. Cryst. Growth*, 53, 337-354. DOI: 10.1016/0022-0248(81)90083-X.

Ogino F., Kawai K., Mayumi K., 1993. Turbulent flow of liquid in a rotating vertical cylindrical container with a stationary solid cylinder at the liquid surface. *9th Symp. on Turbulent Shear Flows, Kyoto, Japan, August 16–18, 1993.* Conference paper 3, 30-1.

Patankar S.V., 1980. *Numerical Heat Transfer and Fluid Flow.* McGraw-Hill, New York.

Quénot G.M., Pakleza J., Kowalewski T.A., 1998. Particle image velocimetry with optical flow. *Exp. Fluids*, 25, 177-189. DOI: 10.1007/s003480050222.

Raffel M., Willert Ch. E., Kompenhans J., 1998. *Particle Image Velocimetry. A Practical Guide*. Springer-Verlag, Berlin.

Ruiz X., Aguilo M., Massons J., Daiz F., 1991. Influence of dynamic boundary condition on the computed flow patterns inside a coaxial rotating disk-cylinder system. *Comp. Fluids*, 20, 387-398. DOI: 10.1016/0045-7930(91)90080-2.

Schouveiler L., Le Gal P., Chauve M.P., 2001. Instabilities of the flow between a rotating and a stationary disk. *J. Fluid Mech*., 443, 329–350. DOI: 10.1017/S0022112001005328.

Sørensen J.N., Christensen E.A., 1995. Direct numerical simulation of rotating fluid flow in a closed cylinder. *Phys. Fluids*, 7, 764-778. DOI: 10.1063/1.868600.

Suchecki W., 2000. The application of digital velocimetry to the visualisation of particle-laden flows. *Zeszyty Naukowe Politechniki Opolskiej*, 60, Mech. 254/2000, Opole, 319-326 (in Polish).

Suchecki W., 2001. Using the methods of optical flow analysis to verify numerical CFD models. *Chem. Eng. Equip.,* 40, 8–12 (in Polish).

Suchecki W., Alabrudziński S., 2003. A metod of correcting flow velocity maps in digital particle image velocimetry, *Chem. Eng. Equip*., 42 (34), 14-20 (in Polish).

Suchecki W., 2006. Study of fluid motion in the tank apparatus equipped with a rotating disc, *Chem. Eng. Equip*. 45, 228–229 (in Polish).

Suchecki W., 2007. *Visualisation of rotary liquid flows using optical tomography*. Zeszyt Monograficzny Politechniki Gdańskiej, 4, Gdańsk, 23-32 (in Polish).

Suchecki W., 2008. Study of suspension flow by segment crystallizer model, In: Suchecki W. (Ed.), *Wybrane zagadnienia przepływu płynów i wymiany ciepła*. Oficyna Wydawnicza Politechniki Warszawskiej, Warsaw, 23-57 (in Polish).

Von Kármán T., 1921. Über laminare und turbulente Reibung. *J. Appl. Math. Mech.,* 1, 233–252. DOI: 10.1002/zamm.19210010401.

Warn-Varnas A., Fowlis W.W., Piasek S., Lee S.M., 1978. Numerical solutions and laser-Doppler measurements of spin-up. *J. Fluid Mech*., 85, 609-639. DOI: 10.1017/S0022112078000828.

Westerweel J. 1993. *Digital particle image velocimetry - theory and application,* Delft, Delft University Press.

Received 29 September 2012
Received in revised form 07 November 2013
Accepted 29 November 2013